








Controlling spin pumping into superconducting Nb by proximity-induced spin-triplet Cooper pairs

A. K. Chan ^{1,2}✉, M. Cubukcu², X. Montiel³, S. Komori³, A. Vanstone^{1,2}, J. E. Thompson ³, G. K. Perkins¹, C. J. Kinane⁴, A. J. Caruana ⁴, D. Boldrin⁵, M. Blamire ³, J. Robinson³, M. Eschrig ⁶, H. Kurebayashi ² & L. F. Cohen ¹✉

Proximity-induced long-range spin-triplet supercurrents, important for the field of superconducting spintronics, are generated in superconducting/ferromagnetic heterostructures when interfacial magnetic inhomogeneities responsible for spin mixing and spin flip scattering are present. The multilayer stack Nb/Cr/Fe/Cr/Nb has been shown to support such currents when fabricated into Josephson junction devices. However, creating pure spin currents controllably in superconductors outside of the Josephson junction architecture is a bottleneck to progress. Recently, ferromagnetic resonance was proposed as a possible direction, the signature of pure supercurrent creation being an enhancement of the Gilbert damping below the superconducting critical temperature, but the necessary conditions are still poorly established. Here, we demonstrate that pumping pure spin currents into a superconductor in the presence of an external magnetic field is only possible when conditions supporting proximity-induced spin-triplet effects are satisfied. Our study is an important step forward for pure spin supercurrent creation, considerably advancing the field of superconducting spintronics.

¹Department of Physics, Blackett Laboratory, Imperial College London, Prince Consort Road, London SW7 2AZ, UK. ²Department of Electronic and Electrical Engineering and London Centre for Nanotechnology, 17-19 Gordon Street, London WC1H 0AH, UK. ³Department of Materials Science & Metallurgy, University of Cambridge, 27 Charles Babbage Road, Cambridge CB3 0FS, UK. ⁴ISIS Facility, STFC Rutherford Appleton Laboratory, Harwell Science and Innovation Campus, Oxon OX11 0QX, UK. ⁵School of Physics and Astronomy, University of Glasgow, Glasgow G12 8QQ, UK. ⁶Department of Physics, University of Greifswald, Wissen Lockt. Seit, Greifswald 1456, Germany. ✉email: k.chan18@imperial.ac.uk; l.cohen@imperial.ac.uk

Superconductor (SC)/ferromagnet (FM) interfaces are of great interest as potential candidates to exploit the spin degree of freedom in superconducting phenomena, leading to potential applications for cryogenic memory and novel computing technologies^{1,2}. As its cornerstone observation, the presence of a spatially varying magnetisation at a SC/FM interface has been found to generate long range spin-polarised triplet supercurrents in the FM via a superconducting proximity effect in combination with spin mixing and spin flip scattering processes^{1,3–10}. These proximity-induced triplet supercurrents are attractive for emerging applications in superconducting spintronics as transmitters of spin information within logic circuits, without incurring ohmic dissipation^{1,3–7,11}.

Creation of pure spin currents within a superconductor would also accelerate developments in the field, particularly if their generation was independent of the Josephson junction architecture. Houzet¹² proposed such a route by using ferromagnetic resonance (FMR). It has been long established that spin pumping is a direct means to generate and transport pure spin currents from a FM into adjacent materials using the magnetisation dynamics [$M(t)$] associated with ferromagnetic resonance^{13–15}. The generation of spin currents from the FM affects the magnetisation dynamics via the enhancement of the effective Gilbert damping α .

Using FMR, it has been demonstrated^{16,17} in FM/SC systems with clean interfaces that the SC blocks the transport of a dynamically driven spin current. The creation of equilibrium (spin-zero) spin-singlet Cooper pairs depletes the number of normal electrons in the SC, and therefore suppresses Andreev reflection at the FM/SC interface. Below T_c , singlet blocking dominates and results in a decrease of α ^{18,19}.

However, recently Jeon et al.²⁰ demonstrated that pure spin currents appeared to survive within superconducting Nb when spin pumping by FMR into Pt/Nb/Py/Nb/Pt stacks, but only when Pt a strong spin-orbit coupling (SOC) layer was included^{20–23}. The identifying feature was a sustained broadening of the FMR linewidth associated with an increase in α , as the sample was cooled below T_c . These observations are consistent with the theoretical predictions that SOC in combination with the ferromagnetic exchange interaction can also generate conditions for the formation of spin triplet superconductivity^{24,25}. Although an important and encouraging development, the influence of the spin triplet channel on the ability to pump pure spin currents into a superconductor was obscured by the non-local character of the Py and Pt interaction, indeed the source of much subsequent discussion^{18,19,26,27}. Therefore, the precise role of the spin triplet channel on pure spin pumping into a superconductor remains an outstanding question.

To explore this research question explicitly, we study a system previously shown to support long range proximity-induced spin triplets. We fabricate a series of samples with 6 nm of Fe to observe the behaviour of superconducting pair states in Nb/Fe/Nb and Nb/Cr/Fe/Cr/Nb structures above and below T_c , as illustrated in Fig. 1. As observed by Robinson et al.^{28,29}, the inclusion of Cr in Nb/Cr/Fe/Cr/Nb structures provide the correct conditions to form proximity-induced spin triplet states through artificially engineered spatially inhomogeneous magnetism. In their Josephson junction measurements, they varied the Fe thickness to characterise the coherence length of the singlet and triplet Cooper pairs. By including a F/F/F type inhomogeneous magnetic layer introduced through the inclusion of Cr, long lived triplet pair states were observed to survive across Fe distances well beyond 6 nm. Measurements of the Fe thickness dependence of the characteristic voltage on Nb/Fe/Nb Josephson junctions show an oscillatory decay³⁰. However, with 6 nm of Fe they showed a similar characteristic voltage as Nb/Cr/Fe/Cr/Nb Josephson junctions. With a fixed Fe thickness of 6 nm in our samples, a

mixture of singlet and triplet pair states are expected, and their behaviour can be compared with the singlet only case of the Nb/Fe/Nb structure. Of course, the Josephson junction experiment probes close-to-equilibrium physics and the decay of a supercurrent within a ferromagnet, whereas the FMR experiment that we propose here is an out-of-equilibrium experiment where spin is pumped from a ferromagnet into a superconductor. In the context of this and previous FMR experiments, the performance of Nb/Fe/Nb and Nb/Cr/Fe/Cr/Nb structures under FMR spin pumping conditions, particularly in the presence of an external magnetic field, is pertinent, timely and has wider implications for the field.

Importantly, we find that in our structures the Fe layer has in-plane uniaxial magnetic anisotropy. This allows us to place a further condition on the spin triplet state survival in finite magnetic fields necessary for FMR resonance. We demonstrate experimentally that when the applied magnetic field lies along the magnetic hard axis, an enhancement of the Gilbert damping persists to low temperatures in Nb/Cr/Fe/Cr/Nb structures, whereas we do not observe this signature when the field lies along the easy. We also show that the Gilbert damping enhancement is absent in Nb/Fe/Nb samples regardless of orientation with respect to the external magnetic field.

Results

All samples were grown on SiO₂/Si(001) where the oxide layer is 250 nm thick. In the main body of the paper, we focus on samples grown with a 6 nm thick layer of Fe and a 31 nm thick layer of Nb, referred to as 31Cr when including a 1 nm thick layer of Cr, and 31NCr when Cr is absent. A range of samples with different Nb thickness have been explored. A summary of these structures is given in Table 1, and the results of these samples are shown and discussed in Supplementary Notes 1–6.

Magnetic characterisation and anisotropy. Although the Fe is polycrystalline, it shows in-plane uniaxial magnetic anisotropy. Figure 2a shows room temperature magnetisation $M(H)$ data taken on sample 31Cr in different in-plane magnetic field orientations showing uniaxial magnetic easy and hard characteristics. This is also confirmed by our FMR measurements. Typical FMR spectra measured along the two directions, shown in Fig. 2b, display a significant difference in FMR resonance field $\mu_0 H_{\text{res}}$. The temperature dependence of $\mu_0 H_{\text{res}}$ for samples 31Cr and 31NCr are shown in Fig. 2c, demonstrating that the anisotropy is sustained to low temperatures. The difference in resonance field $\mu_0 \Delta H_{\text{res}}$ between applying the external dc field along the easy and hard directions is shown in Fig. 2d. H_{res} is higher in the Cr containing film. This behaviour is confirmed in a further series of samples 32Cr, 32NCr, 30Cr and 25Cr (see Supplementary Notes 1 and 2).

The magnetic anisotropy H_k can be extracted from the modified Kittel formula fitted to the FMR data, taken with the dc field applied along the easy and hard magnetic directions^{31–33}, as set out in Eq. 1:

$$f^2 = \left(\frac{\gamma\mu_0}{2\pi}\right)^2 \left[\{M_{\text{eff}} + H_{\text{res}} + H_k \sin^2(\phi - \phi_0) + H_{\text{shift}}^{\text{SC}}\} \times \{H_{\text{res}} - H_k \cos 2(\phi - \phi_0) + H_{\text{shift}}^{\text{SC}}\} \right], \quad (1)$$

where γ is the gyromagnetic ratio, μ_0 is the permeability of free space, M_{eff} is the effective saturation magnetisation, ϕ is the angle of the film's magnetisation with respect to the easy axis magnetic direction, ϕ_0 is the angle of the hard axis direction with respect to the easy axis direction, and $H_{\text{shift}}^{\text{SC}}$ is the contribution to the local field acquired in the superconducting state³⁴ (see Supplementary Note 5 for further details). Due to the relatively small values and

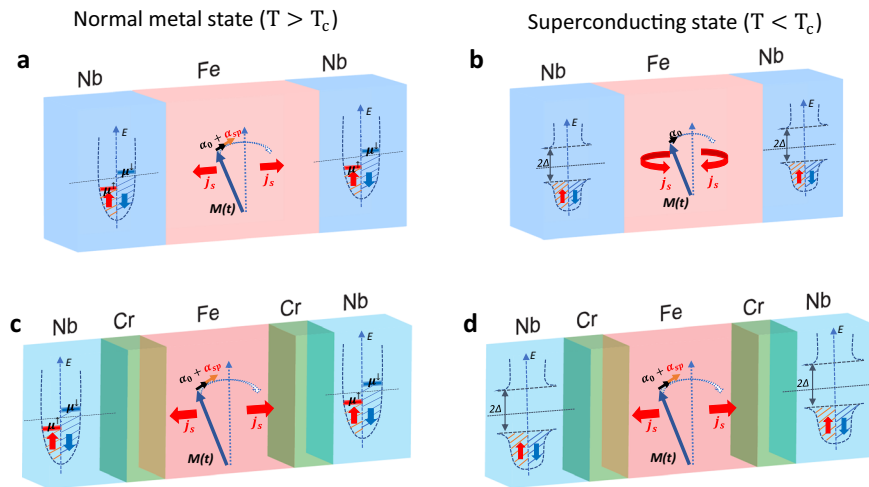


Fig. 1 Schematic diagrams of spin pumping in Nb/Fe/Nb and Nb/Cr/Fe/Cr/Nb heterostructures. Schematics above (a, b) and below (c, d) the critical superconducting transition temperature, T_c , where (d) indicates the formation of triplets with the disorder Fe/Cr spin interface and (c) the lack of triplet generation for the ordered Fe/Nb interface. Spin-dependent density of states and its occupation in superconductors are indicated by the red (majority-spin) and blue (minority-spin) symbols. $M(t)$, J_s and $\alpha_{sp}(\alpha_0)$ represent the time-varying magnetisation vector of the ferromagnet, the spin current injected from the ferromagnet into the superconductor by spin pumping, and the Gilbert damping of the ferromagnet relevant (irrelevant) to the spin pumping, respectively. μ^\uparrow , μ^\downarrow and Δ are the spin dependent electrochemical potentials and superconducting energy gap, respectively.

sensitivity of H_k compared to H_{res} and M_{eff} , we simultaneously fit data taken with the applied magnetic field aligned along the easy and hard axis direction in order to extract single values for H_k and M_{eff} . Example fits for 31Cr and 31Ncr are shown in Fig. 3a and Fig. 3b respectively. It can be observed that the magnetic anisotropy is sustained down to 2 K for a sample with and without Cr. The anisotropy energy constant K can then be calculated by the relation $K = H_k M_s / 2$ and summarised in Table 1. We can observe fair agreement between K extracted from two independent techniques, i.e. $M(H)$ and FMR. Uniaxial magnetic anisotropy has been reported in Fe films angle sputtered onto SiO₂/Si producing sizable structural anisotropy^{35,36}. However, we can rule this out as the source of anisotropy in our films because the Fe in our films are nanocrystalline (confirmed by atomic force microscopy shown in Supplementary Fig. 16) and are grown on a rotating substrate table. Uniaxial magnetic anisotropy is also known to occur in Fe alloys when grown in the presence of an external magnetic field, such as in our case with dc magnetron sputtering^{37,38}. The Fe alloy will experience atomic pair ordering, whereby the Fe atom bonds are elongated along the magnetic field direction. It is known that Nb and Fe can alloy³⁹, and that Cr inter-diffuses into Fe⁴⁰. Therefore, it is likely that atomic pair ordering occurs within the interfacial layers between Fe and Nb and between Fe/Cr and Cr/Nb and is the likely source of the uniaxial magnetic anisotropy observed in our samples. An extended discussion on the source of anisotropy is included in Supplementary Note 8.

Gilbert damping. We observe that the FMR linewidth ΔH has a linear dependence on frequency f , as shown in Fig. 3c. The Gilbert damping α and the inhomogeneous broadening ΔH_0 can be extracted from ΔH vs f plots using the following equation⁴¹:

$$\Delta H = \Delta H_0 + \frac{4\pi\alpha}{\gamma} f. \quad (2)$$

where a number of previous experimental works have shown good agreement between data and this linear relationship^{42–44}. Example fits for sample 31Cr and 31Ncr are shown in Fig. 3c and Fig. 3d respectively. The presence of Cr at the interfaces increases $\mu_0\Delta H_0$ by a factor of two to three (for Nb/Fe/Nb samples

$\mu_0\Delta H_0 \approx 10$ mT and Nb/Cr/Fe/Cr/Nb samples $\mu_0\Delta H_0$ lies between 20 mT and 30 mT) as expected for the increased interfacial magnetic disorder that occurs due to the Cr inter-diffusion at the Cr/Fe interface.

Figure 3e shows α for sample 31Cr as a function of temperature extracted from ΔH , for microwave frequencies from $f = 12$ GHz to $f = 20$ GHz. Note that the α values shown are averaged over several measurements. We also checked the reproducibility of measurements by performing experiments with the microwave stripline placed in different regions of the sample (see Supplementary Note 7)—the error bars reflect the variability in measurement. In-phase ac susceptibility χ'_{ac} (red) measurement of the bulk T_c are plotted on the same graph. The onset of superconductivity is indicated by a decrease in χ'_{ac} , with the gap fully opened when χ'_{ac} reaches a constant minimum value (see Supplementary Note 4 and Supplementary Fig. 8 for further information). For all frequencies, α is almost T -independent between 16 K and T_c . As the temperature is reduced below T_c , a significant temperature-dependent enhancement of α occurs for the field aligned along the hard-axis that is in stark difference from spin transport blocking caused by singlet Cooper pairs^{16–18,26,27}. This clear enhancement of α with Cr samples below T_c is indicative of higher rates of spin relaxation in the Fe layer when the Nb layers are superconducting^{13,14}. Since a spin current carries spin-angular momentum, this damping enhancement that increases as the sample is cooled suggests an increasingly strong spin-current transmission and dissipation as the superconducting gap opens, consistent with previous observations^{20–23}. When the same experiment is repeated for the field aligned along the magnetic easy axis, the sustained enhancement of α is absent, as shown in Fig. 3e. Samples without Cr replicate this latter behaviour below T_c regardless of the orientation of the magnetic field alignment with respect to the easy and hard magnetic axis, as shown in Fig. 3f for sample 31Ncr. These observations are repeated in additional series of samples 32Cr, 32Ncr, 30Cr and 25Cr (see Supplementary Note 3) and the results are consistent with those reported here. Supplementary Notes 9 and 10 also sets out a theoretical model which described a physical scenario that captures some of the essential aspects of the experimental work. However, the physical

Table 1 Samples and their magnetic property values.

Sample Structure	Ref	Easy axis $\mu_0 H_c$ (mT)	Hard axis $\mu_0 H_c$ (mT)	Easy axis M_r/M_s	Hard axis M_r/M_s	M_s (10^3 A/m)	K_{VSM} (J/m ³)	K_{FMR} (J/m ³)
Nb(32)/Cr(1)/Fe(6)/Cr(1)/Nb(32)	32Cr	7.4	1.1	0.93 ± 0.03	0.19 ± 0.01	1680 ± 37	8193 ± 1359	9008 ± 158
Nb(32)/Fe(6)/Nb(32)	32NcR	8.3	3.4	0.90 ± 0.04	0.50 ± 0.02	1500 ± 41	7438 ± 1172	5060 ± 73
Nb(31)/Cr(1)/Fe(6)/Cr(1)/Nb(31)	31Cr	9.8	6.0	0.95 ± 0.04	0.68 ± 0.03	1480 ± 38	5153 ± 748	6030 ± 141
Nb(31)/Fe(6)/Nb(31)	31NcR	9.4	9.0	0.97 ± 0.04	0.79 ± 0.03	1250 ± 37	1348 ± 200	3600 ± 77
Nb(30)/Cr(1)/Fe(6)/Cr(1)/Nb(30)	30Cr	6.7	3.6	0.91 ± 0.03	0.53 ± 0.02	1500 ± 37	4087 ± 713	5470 ± 74
Nb(25)/Cr(1)/Fe(6)/Cr(1)/Nb(25)	25Cr	5.2	2.2	0.88 ± 0.03	0.40 ± 0.01	1410 ± 35	2175 ± 430	4320 ± 71

K_{VSM} and K_{FMR} are the anisotropy constant values obtained from the vibrating sample magnetometer and the ferromagnetic resonance measurements respectively. $\mu_0 H_c$, M_r , and M_s are the coercive magnetic field, the remanent magnetisation and the saturation magnetisation respectively. The error in $\mu_0 H_c$ is ±0.1 mT from measurement precision. The error in M_r is from propagating errors in measuring the Fe volume and saturation moment. The error in K_{FMR} is from the error in the Kittel fits to the frequency dependent resonance magnetic field $\mu_0 H_{res}$.

interpretation of the chosen parameters set cannot be easily mapped to the experiment. Nevertheless, we include the theoretical model in Supplementary Notes 9 and 10 for completeness.

Discussion

Let us consider the various temperature regimes that delineate the key experimental observations. Firstly, above T_c , we find that Cr containing samples have larger ΔH_0 and larger Gilbert damping than the samples without Cr implying that the presence of the Cr always adds an additional spin relaxation channel. Although rather temperature insensitive above T_c , this channel presents a more efficient loss mechanism when the magnetic field is in the hard axis. Together this suggests that Cr creates a strong spin relaxation channel most likely related to a spin misorientation angle between an interfacial disordered Cr/Fe diffused magnetic layer and the spin current polarisation^{13,45}.

At T_c , the onset of superconductivity, in both the non-Cr containing samples and the Cr containing samples with the field along the easy axis, a peak is observed in α . This is associated with the formation of the quasiparticle coherence peak^{18,27,46}. The injected spin current (and therefore the damping) first increases due to the enhanced availability of quasiparticle states just below T_c , and then decreases upon further cooling as the quasiparticle states freeze out and the superconducting gap begins to fully open¹⁷.

Below T_c , $\alpha(T)$ behaves in two different ways depending on the presence of Cr and the field orientation. Regardless of field orientation, samples without Cr show a decrease in α . Similarly, regardless of the Cr layer, measurements with the field applied along the easy axis show a decrease in α . Both scenarios indicate partial spin blocking below T_c due to the onset of superconductivity.

In samples containing Cr when the field is along the hard axis, α increases steadily as the temperature is reduced well below T_c . The ac susceptibility curve marks where the transition to the superconducting state completes. This is a striking difference to the above coherence peak scenario and the observation cannot be attributed to the quasiparticle population^{18,19}. The clear enhancement of α in the Cr samples well below T_c is indicative of higher rates of spin relaxation when the Nb layers are superconducting^{13,14}.

It has been previously reported that trapped flux vortices in a superconducting layer due to an external field can lead to FMR linewidth broadening³⁴. This aspect has been acknowledged in our Kittel fit in Eq. 1 by including the H_{shift}^{SC} term. However, trapped flux vortices cannot be the source of our observed Gilbert damping enhancement. It is expected that trapped flux would occur independent of field orientation. Therefore, if the rise in Gilbert damping is due to trapped flux, we would expect to observe a rise regardless of field orientation. This is not the case in all four samples that exhibit damping enhancement; only when the field is applied in the samples' hard axis orientation do we observe damping enhancement below T_c .

Since a spin current carries spin-angular momentum, this damping enhancement suggests an increasingly strong spin-current transmission and dissipation as the superconducting gap opens, indicative of a spin triplet channel in the Nb. This is consistent with, although significantly larger than, previous observations^{20–23}.

It is already established from Josephson junction measurements (where there is an absence of applied field) that below T_c , the spin misorientation between Fe and the inter-diffused Fe/Cr layer magnetisation produces long-range triplet correlations^{12,47–49}. Here, in the case where an applied field is necessary, we suppose that the misorientation survives most

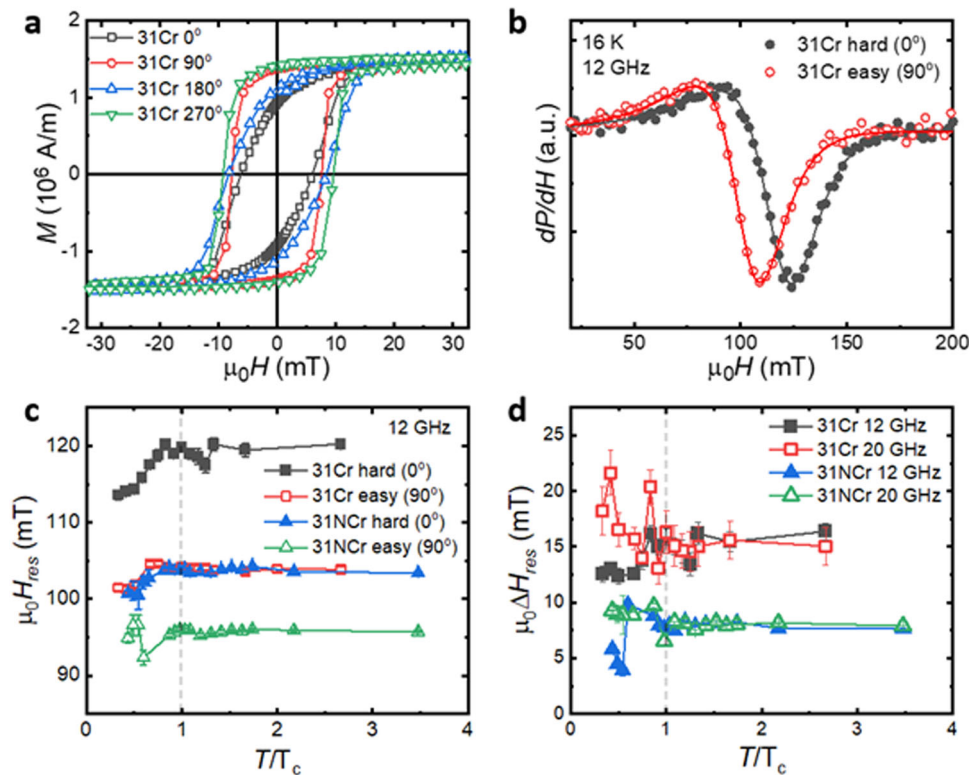


Fig. 2 Magnetisation data for the samples 31Cr and 31NcCr. **a** Magnetic field dependent magnetisation curves $M(H)$ for film 31Cr in four orientations with respect to the applied in-plane field measured at 300 K. **b** Ferromagnetic resonance (FMR) absorption power derivative (dP/dH) for sample 31Cr measured at 16 K. **c** Resonance magnetic field $\mu_0 H_{res}$ as a function of temperature for film 31Cr and 31NcCr extracted from FMR measurements. **d** The temperature dependence of the difference in $\mu_0 H_{res}$ between the hard and easy orientations ($\mu_0 \Delta H_{res}$) for films 31Cr and 31NcCr. Errors for the $\mu_0 H_{res}$ data are from the Lorentzian derivative fitting.

robustly when the field is aligned along the magnetically hard axis^{29,37,50–52}. Of course, we only observe the component of the triplet channel that survives in the dc fields required under the resonance condition. Although the volume magnetisation suggests macroscopic saturation at fields in the tens of mT (Supplementary Fig. 1), evidence from magnetotransport of Cr/Fe multilayers suggests canting of spins at this interface survive to high magnetic fields^{28,40}. The presence of equal-spin Cooper pairs provides a new channel to carry spin within the superconducting Nb where it dissipates due to the inherent spin-orbit coupling in that material. Sample series 31Cr, 30Cr and 25Cr, where the uniaxial magnetic anisotropy is measurably reduced when compared with 32Cr (refer to Table 1 and Supplementary Fig. 1b and c), show a reduced upturn of $\alpha(T)$ along the hard axis (shown in Supplementary Fig. 6). This supports the statement that the introduction of Cr at the interface does not in itself provide a sufficient condition for the spin triplet channel unless the spin misalignment angle between Fe and the interfacial layer can be maintained at the FMR resonance field condition.

To discuss the effect of the uniaxial magnetic anisotropy more quantitatively, we quantify the damping enhancement by introducing parameter S , given by

$$S = \frac{\alpha(0.2t) - \alpha(2t)}{\alpha(2t)}, \quad (3)$$

Where t is the reduced temperature ($t = T/T_c$), such that $\alpha(0.2T_c)$ and $\alpha(2T_c)$ are the Gilbert damping values at $0.2t$ and $2t$ respectively. When the dc magnetic field is applied along the hard axis of our Nb/Cr/Fe/Cr/Nb multilayer stack the spin channel strength created below the superconducting critical temperature is $S = 0.36 \pm 0.05$ for sample 32Cr, $S = 0.18 \pm 0.04$ for sample

31Cr, $S = 0.13 \pm 0.01$ for sample 30Cr, and $S = 0.05 \pm 0.05$ for sample 25Cr (in the SI). To find a possible explanation for the varying S parameters, the anisotropy constant can be plotted as a function of S , shown in Fig. 4a. A clear positive correlation is observed between K and S , indicating that higher magnetic anisotropy is crucial in generating a spin-triplet channel by FMR spin pumping, as the spin misalignment is more readily sustained at the fields required to achieve resonance. K also appears to be dependent on the Nb thickness, as shown in Fig. 4b. However, the reason for this relationship is unclear. An analysis of the S parameter measured in the magnetic easy axis is given in Supplementary Note 6.

The S parameters from our FMR experiment on a S/F/F/F/S structure can be compared to the previous example of Pt/Nb/Py/Nb/Pt²⁰, where the spin-orbit coupling and ferromagnetic exchange were spatially separated, giving $S = 0.066$. The possible higher S values produced by spin pumping into Nb/Cr/Fe/Cr/Nb multilayer stacks suggest that the spin flip and spin scattering processes provided by the single inhomogeneous interface allows for a more efficient means of producing spin-triplet supercurrents in the superconductor—but only when the magnetic anisotropy is high enough. This leads to a possible tunability in spin-triplet channel efficiency by means of manipulating the anisotropy.

To summarise our work, we have systematically investigated spin pumping in Nb/Cr/Fe/Cr/Nb and Nb/Fe/Nb multilayers, with the specific goal to establish the impact of superconducting spin triplets on the spin pumping behaviour. We confirm that under optimum conditions for the existence of proximity-induced superconducting spin triplets, the signature for pure spin pumping into the superconducting Nb, namely a sustained α

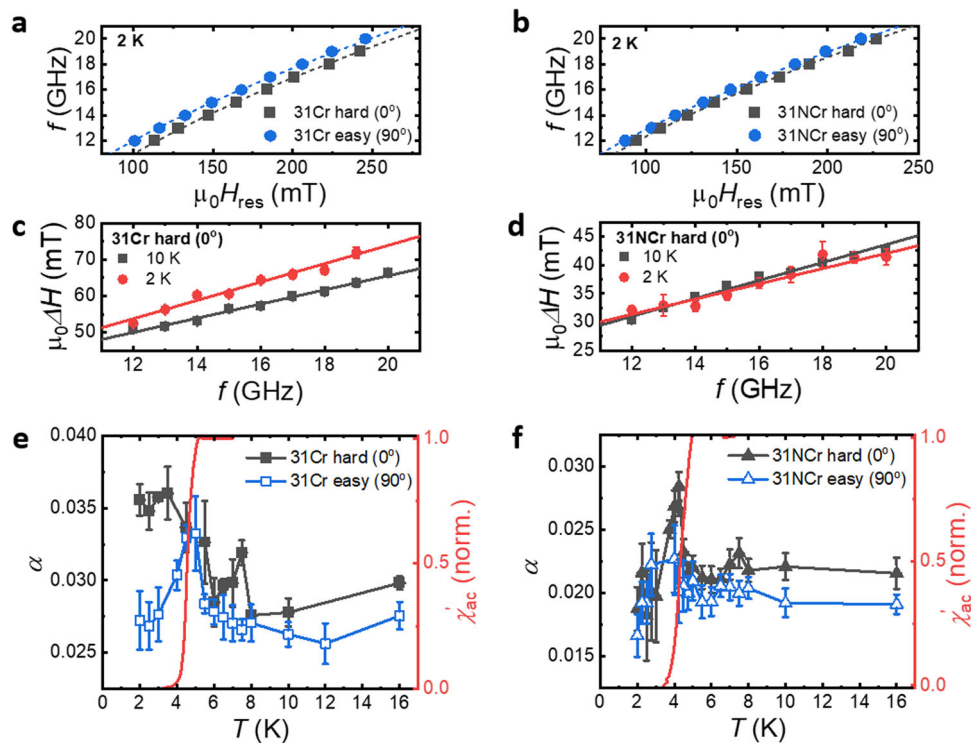


Fig. 3 Parameters extracted from the ferromagnetic resonance (FMR) measurements. Microwave frequency dependence of the resonance magnetic field ($\mu_0 H_{res}$) for sample 31Cr (a) and 31NCr (b), with the field applied in the hard axis orientation (black filled squares) and the easy axis orientation (blue open squares), fitted to a modified Kittel fit (dashed lines) including the anisotropy H_2 and superconducting shift term ($\mu_0 H_{shift}^{SC}$). Microwave frequency dependence of the FMR linewidth ($\mu_0 \Delta H$) for sample 31Cr (c) and 31NCr (d) with the field applied in the hard axis orientation, above (8 K in black) and below (2 K in blue) T_c . Temperature dependence of the Gilbert damping α for sample 31Cr (e) and 31NCr (f) in the hard (filled black symbols) and easy (open blue symbols) orientation. χ_{ac}^i , shown in red, is the in-phase magnetic ac susceptibility. Errors for the α vs T data come from the variability in repeated measurements.

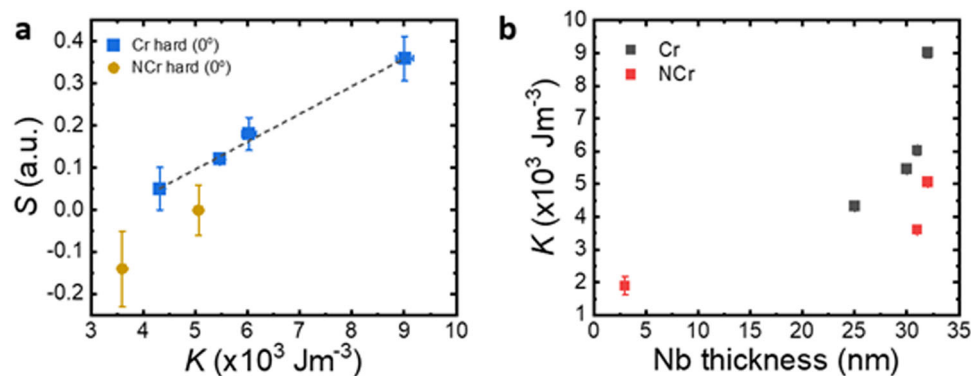


Fig. 4 Anisotropy constant K extracted from the FMR fits at 16 K. a Anisotropy constant K dependence of the S parameter defined as $S = [\alpha(0.2t) - \alpha(2t)]/\alpha(2t)$. The dashed line is a guide to the eye. b Nb thickness dependence of K . The error in S is from propagation of errors. The error in K is from the error in the Kittel fits to the frequency dependent resonance magnetic field $\mu_0 H_{res}$.

enhancement below the superconducting critical temperature, is manifest. These results conclusively show that superconducting pure spin currents can be created within a superconductor under a specific and well-defined set of interfacial conditions. The positive relationship between the anisotropy constant K and the damping enhancement parameter S demonstrate the need for spin misalignment between F²/F² to create a spin-triplet channel. We also highlight that the FMR measurement method itself is a sensitive measure of magnetic relaxation, specifically in relation to spin current emission and dissipation. The damping enhancement parameter S can be used as a relative measure of the strength of spin triplet FMR pumping efficiency between different

types of S/F²/F²/S stacks. Overall, the work accelerates the possibility of utilising spin dependent supercurrents in low loss spintronic applications.

Methods

Sample preparation. The structures were grown on 5 mm × 5 mm SiO₂/Si(001) substrates by d.c. magnetron sputtering in an ultrahigh-vacuum chamber (base pressure of around 10⁻⁸ Pa) with a growth pressure of 1.5 Pa of Ar. Multiple substrates were placed on a rotating circular table that passed in series under stationary magnetrons, so that eight samples

with different layer thicknesses could be grown in the same deposition run. This ensures that the interface properties of the samples presented closely match. The thickness of each layer was controlled by adjusting the angular speed of the rotating table at which the substrates moved under the respective magnetron target and the sputtering power. The thicknesses of Fe and Cr layers were kept constant at 6 nm and 1 nm respectively, while the thickness of the Nb layer varied at 25, 30, 31 and 32 nm.

Superconducting transition measurement. a.c. electrical transport measurements were conducted with a four-point current–voltage method. The resistance R (of a sample) vs temperature T curves were obtained while decreasing T (see supplementary information). From the T derivative of R , dR/dT , the superconducting transition temperature T_c was denoted as the T value that exhibits the maximum of dR/dT .

In-phase a.c. susceptibility measurements were also performed to further confirm T_c when externally dc fields are applied at typical FMR field strengths. Samples are placed within pick up coils with an in-plane drive and external dc fields can be applied in-plane. See SI2 for further information.

Vibrating sample magnetometry. Magnetic field dependent magnetisation curves were taken by a vibrating sample magnetometer (VSM) for the Quantum Design Physical Property Measurement System, with a magnetic resolution of 10^{-6} emu. External dc magnetic fields were applied in-plane to the sample surface. To measure the in-plane anisotropy, samples were rotated by 90° between measurements, and this is done three times for a total of four measurements.

Ferromagnetic resonance. Ferromagnetic resonance (FMR) was performed using a broadband coplanar waveguide (CPW) and ac-field modulation technique. The samples were placed face down on top of the CPWs where an insulator tape is used for electrical insulation. The external dc magnetic field was applied along in-plane direction of the samples, with the rf field also in-plane and fixed perpendicular to the external dc field. The FMR absorption was measured for different frequencies typically ranging from 12 to 20 GHz from room temperature to low temperature at 2K. For each scan, the resonance field (H_{res}) and the half width at half maximum linewidth (ΔH) of the FMR signal were determined by a fit using the field derivative of Lorentzian function (see Supplementary Note 2). To measure the effect of the applied field in-plane direction, samples were rotated by 90° between measurements, and this is done three times for a total of four measurements.

Data availability

The source data that support the findings of this study are available from Prof. H. Kurebayashi (h.kurebayashi@ucl.ac.uk) upon reasonable request.

Received: 14 January 2022; Accepted: 11 September 2023;

Published online: 11 October 2023

References

- Linder, J. & Robinson, J. W. A. "Superconducting Spintronics". *Nat. Phys.* **11**, 307 (2015).
- Yang, G., Ciccirelli, C. & Robinson, J. W. A. "Boosting spintronics with superconductivity". *APL Mater.* **9**, 050703 (2021).
- Singh A., Voltan S., Lahabi K. & Aarts J. "Colossal Proximity Effect in a Superconducting Triplet Spin Valve Based on the Half-Metallic Ferromagnet CrO₂". *Phys. Rev. X*, **5**, 021019 (2015).
- Eschrig, M. "Spin-Polarized Supercurrents for Spintronics". *Phys. Today* **64**, 43 (2011).
- Banerjee, N., Robinson, J. W. A. & Blamire, M. G. "Reversible Control of Spin-Polarized Supercurrents in Ferromagnetic Josephson Junctions". *Nat. Commun.* **5**, 4771 (2014).
- Baek, B., Rippard, W. H., Benz, S. P., Russek, S. E. & Dresselhaus, P. D. "Hybrid Superconducting Magnetic Memory Device Using Competing Order Parameters". *Nat. Commun.* **5**, 3888 (2014).
- Gingrich, E. C. et al. "Controllable 0- π Josephson Junctions Containing a Ferromagnetic Spin Valve". *Nat. Phys.* **12**, 564 (2016).
- Eschrig, M. "Spin polarized supercurrents for spintronics : a review of current progress". *Rep. Prog. Phys.* **78**, 104501 (2015).
- Khair, T. S., Khasawneh, M. A., Pratt, W. P. Jr & Birge, N. O. "Observation of spin-triplet superconductivity in Co-based Josephson junctions". *Phys. Rev. Lett.* **104**, 137002 (2010).
- Klose, C. et al. "Optimization of spin-triplet supercurrent in ferromagnetic Josephson junctions". *Phys. Rev. Lett.* **108**, 127002 (2012).
- Banerjee, N. et al. "Evidence for spin selectivity of triplet pairs in superconducting spin valves". *Nat. Commun.* **5**, 1–6 (2014).
- Houzet, M. "Ferromagnetic Josephson junction with precessing magnetization". *Phys. Rev. Lett.* **101**, 057009 (2008).
- Tserkovnyak, Y., Brataas, A., Bauer, G. E. W. & Halperin, B. I. "Nonlocal Magnetization Dynamics in Ferromagnetic Heterostructures". *Rev. Mod. Phys.* **77**, 1375–1421 (2005).
- Ando, K. et al. "Inverse spin-Hall effect induced by spin pumping in metallic system". *J. Appl. Phys.* **109**, 103913 (2011).
- Mizukami, S., Ando, Y. & Miyazaki, T. "Effect of spin diffusion on Gilbert damping for a very thin permalloy layer in Cu/permalloy/Cu/Pt films". *Phys. Rev. B* **66**, 104413 (2002).
- Bell, C., Milikisyants, S., Huber, M. & Aarts, J. "Spin Dynamics in a Superconductor–Ferromagnet Proximity System". *Phys. Rev. Lett.* **100**, 047002 (2008).
- Morten, J. P., Brataas, A., Bauer, G. E. W., Belzig, W. & Tserkovnyak, Y. "Proximity-Effect-Assisted Decay of Spin Currents in Superconductors". *Europhys. Lett.* **84**, 57008 (2008).
- Silva, M. A. "Large enhancement of spin pumping due to the surface bound states in normal metal–superconductor structures". *Phys. Rev. B* **102**, 180502 (2020).
- Golovchanskiy, I. A. et al. "Magnetization Dynamics in Proximity-Coupled Superconductor-Ferromagnet-Superconductor Multilayers". *Phys. Rev. Appl.* **14**, 024086 (2020).
- Jeon, K.-R. et al. "Enhanced Spin Pumping into Superconductors Provides Evidence for Superconducting Pure Spin Currents". *Nat. Mat.* **17**, 499–503 (2018).
- Jeon, K.-R. et al. "Exchange-field enhancement of superconducting spin pumping". *Phys. Rev. B* **99**, 024507 (2019).
- Jeon, K.-R. et al. "Abrikosov vortex nucleation and its detrimental effect on superconducting spin pumping in Pt/Nb/Ni₈₀Fe₂₀/Nb/Pt proximity structures". *Phys. Rev. B* **99**, 144503 (2019).
- Jeon, K.-R. et al. "Tunable Pure Spin Supercurrents and the Demonstration of Their Gateability in a Spin-Wave Device". *Phys. Rev. X* **10**, 031020 (2020).
- Bergeret, F. S. & Tokatly, I. V. "Singlet-Triplet Conversion and the Long-Range Proximity Effect in Superconductor-Ferromagnet Structures with Generic Spin Dependent Fields". *Phys. Rev. Lett.* **110**, 117003 (2013).
- Bergeret, F. S. & Tokatly, I. V. "Spin-orbit coupling as a source of long-range triplet proximity effect in superconductor-ferromagnet hybrid structures". *Phys. Rev. B* **89**, 134517 (2014).
- Muller, M. et al. "Temperature-Dependent Spin Transport and Current-Induced Torques in Superconductor-Ferromagnet Heterostructures". *Phys. Rev. Lett.* **126**, 087201 (2021).
- Yao, Y. et al. "Probe of spin dynamics in superconducting NbN thin films via spin pumping". *Phys. Rev. B* **97**, 224414 (2018).
- Robinson, J. W. A., Banerjee, N. & Blamire, M. G. "Triplet pair correlations and nonmonotonic supercurrent decay with Cr thickness in Nb/Cr/Fe/Nb Josephson devices". *Phys. Rev. B* **89**, 104505 (2014).
- Komori, S. et al. "Spin-orbit coupling suppression and singlet-state blocking of spin-triplet Cooper pairs". *Sci. Adv.* **7**, eabe0128 (2021).
- Piano, S., Robinson, J. W. A., Burnell, G. & Blamire, M. G. "0- π oscillations in nanostructured Nb/Fe/Nb Josephson junctions". *Eur. Phys. J. B* **58**, 123–126 (2007).
- Kurebayashi, H. et al. "Uniaxial anisotropy of two-magnon scattering in an ultrathin epitaxial Fe layer on GaAs". *Appl. Phys. Lett.* **102**, 062415 (2013).
- Kittel, C. "On the theory of ferromagnetic resonance absorption". *Phys. Rev.* **73**, 155 (1948).

33. Farle, M. "Ferromagnetic resonance of ultrathin metallic layers". *Rep. Prog. Phys.* **61**, 755 (1998).
34. Jeon, K.-R. et al. "Effect of Meissner screening and trapped magnetic flux on magnetization dynamics in thick Nb/Ni80Fe20/Nb trilayers". *J. Phys. Appl.* **11**, 014061 (2019).
35. Komogortsevab, S. V., Varnakovac, S. N., Satsukal, S. A., Yakovleva, A. & Ovchinnikov, S. G. "Magnetic anisotropy in Fe films deposited on SiO₂/Si(001) and Si(001) substrates". *J. Magn. Magn. Mater.* **351**, 104–108 (2014).
36. Westerstrand, B., Nordblad, P. & Nordborg, L. "The Magnetocrystalline Anisotropy Constants of Iron and Iron-silicon Alloys". *Phys. Scr.* **11**, 383–386 (1975).
37. Belyaev, B. A., Izotov, A. V., Skomorokhov, G. V. & Solovev, P. N. "Experimental study of the magnetic characteristics of nanocrystalline thin films: the role of edge effects". *Mat. Res. Express* **6**, 116105 (2019).
38. Diaz, J. et al. "Atomic pair ordering and magnetic anisotropy of Fe–Si amorphous films studied by linearly polarized EXAFS". *J. Magn. Magn. Mater.* **316**, e390–e392 (2007).
39. Balam, S. & Paul, A. "Interdiffusion study in the Fe-Nb system". *Metall. Mater. Trans. A* **41**, 2175–2179 (2010).
40. Ali, S. R. et al. "Role of interface alloying in the exchange bias of Fe/Cr bilayers". *Phys. Rev. B* **82**, 020402 (2010).
41. McMichael, R. D. & Krivosik, P. "Classical model of extrinsic ferromagnetic resonance linewidth in ultrathin films". *IEEE Trans. Magn.* **40**, 2–11 (2004).
42. Rojas-Sánchez, J. C. et al. "Spin pumping and inverse spin Hall effect in germanium". *Phys. Rev., B* **88**, 064403 (2013).
43. Twisselmann, D. J. & McMichael, R. D. "Intrinsic damping and intentional ferromagnetic resonance broadening in thin Permalloy films". *J. Appl. Phys.* **93**, 6903–6905 (2003).
44. Heinrich, B. et al. "Temperature and frequency dependence of microwave magnetic properties of amorphous Fe_{100-x}B_x". *J. Appl. Phys.* **55**, 1814–1816 (1984).
45. Brataas, A., Bauer, G. E. W. & Kelly, P. J. "Non-collinear magnetoelectrics". *Phys. Rep.* **427**, 157 (2006).
46. Inoue, M., Ichioka, M. & Adachi, H. "Spin pumping into superconductors: A new probe of spin dynamics in a superconducting thin film". *Phys. Rev. B* **96**, 024414 (2017).
47. Eschrig, M. "Scattering problem in nonequilibrium quasiclassical theory of metals and superconductors: General boundary conditions and applications". *Phys. Rev. B* **80**, 134511 (2009).
48. Eschrig, M. et al. "Singlet-triplet mixing in superconductor-ferromagnet hybrid devices". *Advances in Solid State Physics*. 533–545. (Springer, Berlin, Heidelberg, 2004).
49. Bergeret, F. S., Volkov, A. F. & Efetov, K. B. "Odd triplet superconductivity and related phenomena in superconductor-ferromagnet structures". *Rev. Mod. Phys.* **77**, 1321 (2005).
50. Montiel, X. & Eschrig, M. "Generation of pure superconducting spin current in magnetic heterostructures via nonlocally induced magnetism due to Landau Fermi liquid effects". *Phys. Rev. B* **98**, 104513 (2018).
51. Simensen, H. T., Johnsen, L. G., Linder, J. & Brataas, A. "Spin pumping between noncollinear ferromagnetic insulators through thin superconductors". *Phys. Rev. B* **103**, 024524 (2021).
52. Montiel, X. & Eschrig, M. "Spin current injection via equal-spin Cooper pairs in ferromagnet/superconductor heterostructures". *Phys. Rev. B* **107**, 094513 (2023).

Acknowledgements

This work was supported by the EPSRC Programme Grant EP/N017242/1, EPSRC Centre for Doctoral Training in Advanced characterisation of Materials Grant EP/L015277/1, and The Leverhulme Trust RPG-2016-306.

Author contributions

A.K.C., H.K., M.C., J.R. and L.F.C. conceived the experiment. The samples presented in this paper were prepared by S.K. and J.E.T.. FMR and VSM measurements were carried out by A.K.C., M.C., and A.V.. AFM measurements were carried out by A.K.C.. AC susceptibility measurements were carried out by A.K.C. and G.K.P.. NPR measurements (Supplementary Note 8) were carried out by C.J.K., A.J.C., and D.B.. Data analyses were carried out by A.K.C., M.C., A.V., C.J.K., A.J.C., D.B., M.B., J.R., H.K., and L.F.C.. Theoretical model calculations (Supplementary Notes 9 and 10) were performed by X.M. and M.E. All authors discussed the results and paper. The paper was written by A.K.C., M.C., H.K., and L.F.C.

Competing interests

The authors declare no competing interests.

Additional information

Supplementary information The online version contains supplementary material available at <https://doi.org/10.1038/s42005-023-01384-w>.

Correspondence and requests for materials should be addressed to A. K. Chan or L. F. Cohen.

Peer review information *Communications Physics* thanks the anonymous reviewers for their contribution to the peer review of this work.

Reprints and permission information is available at <http://www.nature.com/reprints>

Publisher's note Springer Nature remains neutral with regard to jurisdictional claims in published maps and institutional affiliations.



Open Access This article is licensed under a Creative Commons Attribution 4.0 International License, which permits use, sharing, adaptation, distribution and reproduction in any medium or format, as long as you give appropriate credit to the original author(s) and the source, provide a link to the Creative Commons licence, and indicate if changes were made. The images or other third party material in this article are included in the article's Creative Commons licence, unless indicated otherwise in a credit line to the material. If material is not included in the article's Creative Commons licence and your intended use is not permitted by statutory regulation or exceeds the permitted use, you will need to obtain permission directly from the copyright holder. To view a copy of this licence, visit <http://creativecommons.org/licenses/by/4.0/>.

© The Author(s) 2023